Spin dynamics and criteria for onset of exchange bias in superspin glass Fe/γ-Fe_{2}O_{3} core-shell nanoparticles

Sayan Chandra, H. Khurshid, Wanfeng Li, G. C. Hadjipanayis, M. H. Phan, and H. Srikanth

Phys. Rev. B **86**, 014426 — Published 25 July 2012

DOI: 10.1103/PhysRevB.86.014426

Spin dynamics and criteria for onset of exchange bias in superspin glass Fe/γ-Fe_2O_3 core-shell nanoparticles

Sayan Chandra,[1] H. Khurshid,[1, 2] Wanfeng Li,[2] G. C. Hadjipanayis,[2] M. H. Phan,[1] and H. Srikanth[1]
[1]Department of Physics, University of South Florida, Tampa, FL 33620, USA
[2]Department of Physics and Astronomy, University of Delaware, Newark, DE 19711, USA

A detailed study is presented on Fe/γ-Fe_2O_3 core-shell structured nanoparticles (mean size ~ 10 nm) to understand the spin dynamics of the core and shell independently and their role in triggering exchange bias (EB) phenomenon. The particle dynamics critically slow down at T_g ~68 K below which they exhibit memory effect in FC and ZFC protocols associated with a superspin glass state (SSG). The field dependence of mean blocking temperature fits the de Almeida-Thouless line and shows two different linear responses in the low and high field regimes corresponding to the core and shell respectively. We show that the energy barrier distribution estimated from the temperature decay of isothermal remanent magnetization shows two maxima that marks the freezing temperatures of the core ($T_{f\text{-}cr}$ ~48 K) and shell ($T_{f\text{-}sh}$ ~21 K). Lastly, hysteresis measurements after field cooling reveal strong EB indicated by a loop shift associated with unidirectional anisotropy. The onset of EB is at 35 K when the ferromagnetic core is frozen and the moments in the ferrimagnetic shell begin to block resulting in enhanced exchange coupling.

I. INTRODUCTION

The phenomenon of exchange bias (EB) has generated a lot of research interest over the last five decades[1-7]. EB has been reported in thin films with a conventional ferromagnet (FM)-antiferromagnet (AFM) interface[8]; and also in other magnetic nanostructures having ferrimagnetic (FIM) domains[9], spin glasses[10] or surface spin disorder[11]. In the case of thin films, the origin of EB is well understood and is attributed to the unidirectional anisotropy developed at the FM-AFM interface due to pinning of magnetic moments. Recent experiments have also demonstrated EB in the case of samples having a FM layer in contact with a spin glass layer[12, 13]; layered nanoparticle/ferromagnetic structures where various

models have been suggested to explain the origin of EB[14]. Core-shell nanoparticles with a conventional FM (core)/AFM (shell) and more recently "inverted" AFM (core)/FM (shell) have also been studied and the general consensus to explain EB is the freezing of interfacial spins or the growth of droplets with uncompensated spins[15-17].

Usually, core-shell nanoparticles are composed of different materials. Hence we can say that the effective anisotropy, lattice strain, number of uncompensated spins etc. for the materials making up the core and shell are different, which in turn implies that these two materials may have separate responses to change in temperature and magnetic field. So a very fundamental and important question emerges: Can the dynamic and static response of the core and shell be identified separately? While several research efforts have been devoted in understanding the role of interfacial spins in nanoparticles that exhibit EB, a clear understanding of the spin dynamics of the core and shell and their impact on EB remains to be investigated.

In this paper, we have systematically demonstrated that it is possible to identify the individual responses of the core and shell. The system in the present study is ~ 10 nm Fe/γ-Fe_2O_3 nanoparticles. We have shown that the nanoparticles collectively behave like a superspin glass and exhibit distinguishably different magnetic responses of the core and shell. Our findings emphasize that by understanding the magnetic state of core and shell and their interdependence at the onset of EB, it may be possible to appropriately select different materials for core and shell to enhance and suitably tailor EB for applications.

II. EXPERIMENT

The core-shell structured nanoparticles were prepared by high temperature reduction of iron pentacarbonyl in octadecene in the presence of olyelamine (OY) and trioctyl phosphine (TOP), details of which have been published[18]. Briefly, OY and TOP (molar ratio 1:1) were dissolved in octadecene in a three neck flask and heated in an airtight atmosphere while continuously purging with Ar+5%H_2 to get rid of any free oxygen dissolved in the solvent and surfactants. $Fe(CO)_5$ was injected at 220 ^oC and refluxed for one hour to yield a dark solution. The nanoparticles were precipitated and extracted by adding absolute ethanol solution followed by centrifuging. The black powder obtained on drying was tightly packed on Kapton tape.

The structural and microstructural studies were performed using JEOL JEM 3010 FX Transmission Electron Microscopy (TEM). The magnetic properties were carried out using a Quantum Design Physical Properties Measurement System (PPMS) with a vibrating sample magnetometer (VSM) option over a temperature range of 5 – 300 K and applied fields up to 50 kOe.

III. RESULTS AND DISCUSSION

Figure 1a shows a conventional bright field TEM image of these nanoparticles along with a selected area diffraction pattern in the inset. The average size of the nanoparticles is determined to be 9.8 ± 0.7 nm. Contrast variation at the interface clearly suggests a core and shell morphology in these nanoparticles. HRTEM images (Figure 1(b,c)) reveal the crystalline structure of both core and shell, with the lattice spacing of the core and shell corresponding to the (110) planes of bcc iron and (311) planes of fcc iron oxide, respectively. The Fe core is single crystalline; however, the shell of γ-Fe_2O_3 is composed of small crystallites which are oriented randomly[19]. In the inset of Figure 1(a), the selected area diffraction pattern is indexed to bcc iron and fcc iron-oxide. Since the particles lying on the TEM grid have no particular orientation with respect to the incident electron beam (unlike the case of thin films), the electron diffraction pattern for single crystalline core contains (211), (200) and (110) peaks[18].

The nanoparticles have been tightly packed to avoid any physical motion relative to each other. Due to this tight packing, it can be safely concluded that adjacent nanoparticles touch each other with the presence of surfactant layers between them. Hence, the distance between the centers of two adjacent nanoparticles is estimated to be about 10 nm. Figure 2 presents the temperature variation in magnetization (M) measured in 50 Oe under the zero-field cooled (ZFC), field cool warming (FCW) and field cooled cooling (FCC) protocols. During the FCC and FCW measurements, the sample was cooled under an applied field of 50 Oe. The ZFC curve shows a conventional peak ($T_{P\text{-}ZFC}$ ~ 69K) which has been reported in many superparamagnetic (SPM) and superspin glass (SSG) systems that are ferromagnetic in the ground state[20-22]. The peak in ZFC curve for monodispersed, non-interacting particles, is called the blocking temperature (T_B) and is found to occur when the thermal energy (k_BT) is comparable to the activation energy (ΔE_A=KV)[23]. However, the scenario is quite different for

interacting particles with finite size distribution. Recent experiments have shown an increase in temperature along with broadening of the peak of ZFC curve due to enhanced interactions in the nanoparticles[24]. In the present case, there exists irreversibility in the ZFC and FCW curves even at room temperature, which suggests the presence of inter-particle interactions or some particles in the blocked state. Due to the core-shell structure, the nature of interaction and hence the energy barrier is largely controlled by the relative strength of exchange anisotropy, dipole-dipole interaction, surface spin disorder etc. Hence, the peak ($T_{P\text{-}ZFC}$) cannot be termed as the true blocking temperature of the system. Another method for determining the mean blocking temperature (T_B) has been adopted which is discussed later. In the FCW curve, a decrease in magnetization is observed with lowering the temperature below ~ 50 K as shown in the inset of Figure 2(a). It has been reported earlier that the FCW magnetization monotonically increases with decreasing temperature for SPMs, while it tends to saturate to a constant value or even decrease with decreasing temperature for SSGs[20]. This feature in the FCW curve gives us a first indication that the nanoparticles show a collective glassy behavior at low temperature. There also exists a thermal hysteresis in the FCW and FCC curves below ~68K. The onset of thermal hysteresis is marked by a sharp rise (~ T_g) in $M_{FCC} - M_{FCW}$ as shown in inset (b). Such thermal hysteresis has been reported in different systems and may occur due to various phenomena such as kinetic arrest[25], phase transition of first order[26] or due to the presence any thermal memory in the sample which is strongly influenced by the starting state of the system[27]. In our sample, which constitutes of Fe(core)/γ-Fe_2O_3(shell), no such kinetic arrest or first order transition is known for either materials in that temperature range and hence they can be safely ruled out as reasons for thermal hysteresis. This indicates that one of the reasons for thermal hysteresis can be a cooperative effect in the system which also has a thermal memory. The above mentioned features raise an important question about the strength and dynamics of interactions in the nanoparticles.

To probe the spin dynamics of these nanoparticles, ac susceptibility measurements were systematically performed on the sample by applying an ac magnetic field of 10 Oe within the frequency (f) range of 10 Hz to 10 kHz. An ensemble of interacting particles can dominate over single particle blocking that may lead to a collective freezing. By changing the frequency, we are deliberately changing the probe time ($\tau = 1/f$) which allows to probe the

relaxation of particles in different time windows. In the inset of Figure 3a, the frequency dependence of the real part of ac susceptibility (χ') is shown. The peak temperature (T_P) shifts to higher values as frequency increases, which is consistent with other reports[9, 10]. A systematic investigation of the evolution of peak shift in χ' is carried out. The peak shift in χ' can be quantified by Eq.(1) and it is empirically known that for SPM systems, Γ ranges from 0.1 to 0.13 whereas for SSG systems[28] Γ < 0.06. For our system, Γ is estimated to be 0.044 which suggests that our nanoparticles may be SSG type.

$$\Gamma = \frac{\Delta T_P}{T_P \Delta(\log \omega)} \qquad (1)$$

An attempt to fit to Neel Arrhenius (NA) law yielded unphysical results as expected. This clearly indicates that the dynamics of these nanoparticles cannot be explained with a non-interacting particle model. Thus we extended our analysis to the Vogel Fulcher (VF) model which takes into account weak inter particle interactions. According to the VF model, the relaxation time of an ensemble of weakly interacting nanoparticles follows Eq. (2).

$$\tau = \tau_o^{VF} \exp\left[\frac{E_a}{k_B(T-T_o)}\right] \qquad (2)$$

Here, E_a is the anisotropy energy barrier or the activation energy (KV) and τ_o^{VF} is the relaxation time of individual nanoparticle. The term T_o is the characteristic temperature which gives a qualitative measure of the inter particle interaction energy. The obtained fitted (Figure 3a) parameters have reasonable values of E_a/k_B = 571 K, τ_o^{VF} = 6.9 x 10^{-13} s and T_o = 48 K. This successful fit confirms the presence of weak interactions in the nanoparticles that undergo collective freezing at T_o ~ 48 K, henceforth referred to as freezing temperature (T_f). This is in good agreement with the low temperature feature seen in the FCW curve (Figure 2, inset a). For SPM particles[23], the relaxation time τ_o^{VF} is in the range 10^{-8} to 10^{-13} s. The fact that these nanoparticles fall in this range (~10^{-13} s) indicates that they individually relax like SPM particles above the blocking temperature; however, in order to understand their collective behavior, the peak temperatures T_P is fitted to a critical power law (Eq. 3)

$$\tau = \tau_o^{SC} \exp\left[\frac{T}{T_g} - 1\right]^{-zv} \qquad (3)$$

where T_g is the static spin glass temperature which marks the onset of critical slowing and collective glassy behavior; zv is the dynamical critical exponent which is related to the

correlation length ξ that diverges at T_g. The use of such phenomological activation law is usually done for cluster glass magnetic systems, especially SSG[29]. It is known from literature that for a SSG system[29-31], the value of τ_o^{SC} ranges between 10^{-6} to 10^{-9} s. The obtained fit parameters for our nanoparticles are τ_o^{SC} = 2.8 x 10^{-7} s, T_g = 68 K and zv = 3.8. The value of zv is very close to that calculated for 3D Ising model[30] and the value of τ_o^{SC} further strengthens the case for SSG type of behavior. It is to be noted here that the values of τ_o^{VF} obtained from VF model and scaling law are different; in case of the VF model, τ_o^{VF} represents non critical flip time for individual particles, whereas from the scaling law (τ_o^{SC}), we get the time scale for critical slowing down of collective particle relaxation. The glass transition temperature (T_g) is 68 K which is below $T_{P\text{-}ZFC}$ ~ 70 K, suggesting that the glassy behavior of *superspins* closely follows the onset of blocking in the particles. This also explains the development of thermal hysteresis and its progressive enhancement below 68K (Figure 1). These results indicate that the nanoparticles show glassy behavior below T_g that may be SSG type and below T_f ~ 48 K they collectively freeze.

To further elucidate these intriguing features, we performed memory effect in the FC aging protocol and the results are presented in Figure 4a. The sample was field cooled in an applied field of 50 Oe from 300 K to 5 K with intermittent stops (IS) at 90 K, 75 K, 50 K, 35 K and 15 K. At each IS, the field was turned off for t_w = 10^4 s and was turned back on during further cooling process. This is shown by the M_{FC-DN}^{IS} curve. Then the sample was warmed in 50 Oe field from 5 K to 300K without stopping shown by M_{FC-UP}^{IS}. The FCW curve is shown for reference. In the M_{FC-DN}^{IS} curve, a drop in magnetization is observed at every IS as the magnetic moments equilibrate; however, it is seen that the amount of drop depends on the magnetic state of the nanoparticles. After a waiting time t_w, when the field is turned on, the amount of recovery in magnetization (M) depends on how fast the nanoparticles realign to the applied field. So, at temperatures below the T_g (50 K and 30 K), due to the critically slow dynamics of the system, the recovery is less; hence, the observed drop in M is appreciable. It is to be noted here that at 15 K, the drop is relatively less. Also, there is an upturn in M_{FC-DN}^{IS} curve below 15 K. Both these features can be attributed to the freezing of spins in the shell which is discussed later. Above T_g, (90 K, and 75 K) the nanoparticles do not show collective behavior and hence most of the drop in M is recovered when the field is turned on before further cooling. In the M_{FC-UP}^{IS} curve, it is seen that on warming, the

magnetization exhibits step like features at every IS. Such a phenomenon has been observed in nanoparticles irrespective of their strength of inter particle interaction and is attributed to a distribution in energy barrier[32, 33]. In the cooling process, at every IS, a certain amount of *dynamically active* nanoparticles with volume close to the blocking volume equilibrate and remain blocked on subsequent field cooling. So, at an IS in the cooling process, the magnetic moment configuration of the ensemble of nanoparticles is imprinted in its "memory". This is retrieved in the warming process which results in the step like feature in M_{FC-UP}^{IS} curve[32]. We can conclude that the FC memory effect is more dominant below T_g when the dynamics of the nanoparticle ensemble critically slows down. In addition, the fact that the magnetization in field cooled curves is decreasing with decreasing temperature suggests that the system is SSG like.

A peculiar test of SSG is aging effect in the ZFC protocol which is absent in the case of SPM particles[32]. In the single stop wait (SSW) protocol, the sample was cooled to 5 K under zero field with an intermittent stop (IS) at 50 K for 10^4 s. Then the magnetization was measured on warming (M_{ZFC}^{SSW}) under an applied field of 50 Oe. The difference in magnetization ($M_{ZFC}^{SSW} - M_{ZFC}^{ref}$) is plotted in Figure 4b, where M_{ZFC}^{ref} is the magnetization measured under ZFC protocol without stopping. A peak in $-(M_{ZFC}^{SSW} - M_{ZFC}^{ref})$ is seen at IS temperature (~ 50 K) which is a signature of a SSG system and its origin can be understood from the droplet model proposed by Fisher et. al.[34, 35]. According to the droplet model, a spin glass domain can be thought of as a droplet or a cluster whose volume increases with time because of the non-equilibrium nature of dynamics. In the SSW process as the droplet volume increases with time at 50 K, so does the mean energy barrier[34, 35]. But, in the reference ZFC case, the energy barrier of the droplets at 50K is relatively lower. During the warming process, it is known that the flip of clusters is governed by thermal activation. This means that M_{ZFC}^{ref} will be greater than M_{ZFC}^{SSW} at 50K, because the *superspin* clusters associated with the reference ZFC cooling protocol are smaller and flip below 50 K rendering higher magnetization than the bigger clusters formed in the SSW protocol that flip at higher temperature. This difference in magnetization at 50 K is seen as the peak in figure 4b. It can be conclusively inferred that below T_g, the core-shell nanoparticles show aging and are of SSG type.

In view of our understanding of the system from the preliminary dc and ac magnetization results, two important inferences can be drawn; (i) the nanoparticles show cooperative behavior similar to SSG below T_g and (ii) there exist inter particle interactions in the SPM state that are dominant enough to maintain irreversibility in the ZFC-FCW curves even at RT. So, as the temperature increases, the nanoparticles go from SSG to SPM state with finite interactions. In the case of granular thin films of FM nanoparticles embedded in a matrix, there have been studies indicating crossover from SSG to superferromagnet (SFM) with increasing concentration of FM nanoparticles[36]. It has also been demonstrated that for lower concentration of FM nanoparticles, the SSG system goes into the interacting superparamagnet (ISPM) regime[37, 38]. *Now the question that arises is, at what temperature does the crossover from SSG to SPM occur in the present system?* The answer to this is rather non trivial. Usually an ensemble of nanoparticles is said to be in the SPM state above the blocking temperature identified as the temperature corresponding to the peak in ZFC curve. This is true for mono disperse nanoparticles with negligible or no interactions. But, in the case of nanoparticles with finite size distribution, there is always a precursor effect associated with unblocking of smaller particles at temperatures lower than $T_{P\text{-}ZFC}$. Moreover, the presence of inter particle interactions, and the formation of clusters further shift $T_{P\text{-}ZFC}$ to higher temperature. In the case of core-shell nanoparticles, since the core and shell are composed of different materials, they have different magneto crystalline anisotropy, thermal activation, uncompensated spins, lattice strain etc. Hence, all these factors together suggest that $T_{P\text{-}ZFC}$ may not be the true blocking temperature, at least in case of core-shell nanoparticles. We define the mean blocking temperature ($\langle T_B \rangle$) as the temperature corresponding to the fastest change in the separation of ZFC from FCW curve, which, in turn is associated with the maximum number of nanoparticles unblocking as the temperature increases[39]. This can be easily determined by identifying the peak position in $\frac{d(M_{FCW}-M_{ZFC})}{dT}$. Figure 5a shows the M(T) curves (left axis) measured at 100 Oe indicating the peak in ZFC curve ($T_{P\text{-}ZFC}$), while on the right axis, $-\frac{d(M_{FCW}-M_{ZFC})}{dT}$ is plotted against temperature whose peak marks $\langle T_B \rangle$ as defined above.

In order to study the effect of applied field on $\langle T_B \rangle$, M(T) measurements were conducted under the ZFC and FCW protocols in magnetic fields ranging from 50 Oe to 20 kOe. Generally, in the case of single domain particles, the blocking temperature

monotonically shifts to lower temperatures due to lowering of energy barrier on the application of magnetic field. Theoretically, the blocking temperature should decrease with the increasing applied field and eventually disappear when the field reaches a critical value; however, the rate of decrease in blocking temperature is strongly controlled by anisotropy[40], dipole-dipole interaction[41] and volume fraction of disordered spins. The inset of Figure 5b shows the dependence of $<T_B>$ on applied field. In the low field regime, $<T_B>$ decreases sharply and above ~6 kOe, the decrease is gradual. The presence of two slopes suggests that the distribution of energy barrier is bimodal; one that is affected at low fields and another one at high fields. In the case of the core-shell nanoparticles, we have a single crystalline core and a shell composed of randomly oriented magnetic domains (Figure 1c). It has been reported that the effective anisotropy for hollow γ-Fe_2O_3 is about ~ 8 x 10^5 J/m^3 which is more than 5 times that of Fe nanoparticles[42, 43] (~ 1.3 x 10^5 J/m^3). This means that the mean energy barrier associated with the core (E_{cr}) is lower than the one for the shell (E_{sh}). The rate of decrease in $<T_B>$ is affected by the relative suppression of E_{cr} and E_{sh} in the low and high field regimes. In the low field regime, E_{cr} is suppressed more while E_{sh} remains unaffected which implies that the response of $<T_B>$ to field (sharp decrease) is predominantly influenced by the core. But, above a critical field, when the moments in the core are fully aligned, suppression of E_{sh} mainly contributes to the decrease in $<T_B>$. In case of nanoparticle systems, the presence of dipolar interaction has significant influence on the magnetic properties as it modifies the anisotropy energy barrier of individual particles thereby modifying the evolution of glassy dynamics[44], and blocking temperature[41]. The evolution of $<T_B>$ can be mapped on the H-T plane in order to distinguish the glassy phase from the SPM phase. From mean field theory, it is predicted that the existence of glassy behavior for a fixed temperature will be destroyed above a critical field[30, 45]. Two such critical lines were proposed by Almeida Thouless (AT line) and Gabay Thouless (GT line) for anisotropic Ising spins and for isotropic Heisenberg spins, respectively[45]. The AT line behaves as $< T_B > \propto H^{2/3}$ while the GT line behaves as $< T_B > \propto H^2$. Later it was shown by numerical calculations that such critical lines can exist in nanoparticles marking the transition from glassy to SPM behavior[46]. Figure 5b shows that the variation in $<T_B>$ follows the AT line in both the low field and high field regimes. Attempts to fit the GT line yielded straight lines in both low and high field regimes, but with lower regression values compared to AT line. The fit is consistent with our calculations of zv from scaling law confirming that

the system is indeed composed of Ising type spins. We can infer that the nanoparticles behave like SSG to the left of the AT line and SPM to the right. The y-intercept of the low field regime fit is ~57 K which can be attributed to the mean blocking temperature of the core at H=0 (T_{B1}). Similarly, the y intercept of the high field regime fit ~24 K corresponds to the mean blocking temperature of the shell at H=0 (T_{B2}). It has been reported in other systems that the critical behavior crosses over from AT line to GT line when the applied field is greater than the anisotropy field[47, 48]. In the case of our core-shell nanoparticles, along with the presence of unidirectional random anisotropy, the exchange anisotropy is so high that such a crossover is not observed. This is supported by the fact that even at fields up to 20 kOe, irreversibility is observed between the ZFC and FCW curves.

From the above discussion, it is rather intriguing to estimate the temperature dependence of energy barrier. It was shown that the distribution in energy barrier can be mapped out from the temperature decay of remanence[49]. The remanent magnetization is related to the blocking temperature distribution function by Eq.(4).

$$I_r(T) = \alpha M_s \int_T^{\infty} f(T_B) dT_B \qquad (4)$$

Here, α is a constant that takes into account the random orientation of anisotropy in the nanoparticles[50], and M_s is the saturation magnetization. The blocking temperature distribution function $f(T_B)$ can be measured from the derivative of Eq. (4) i.e., $\frac{dI_r}{dT} \propto f(T_B)$. The function $f(T_B)$ represents the distribution of energy barrier. It is to be noted that the distribution function $f(T_B)$ should not be confused with the mean blocking temperature $\langle T_B \rangle$. The measurement protocol was to expose the sample to a high field at a constant temperature; turn the field off and then measure the magnetization. Figure 6a shows the temperature dependence of remanent magnetization. As the temperature decreases, the remanent magnetization increases like in a conventional ferromagnet until ~35 K, below which an unusual decrease is seen. The remanent magnetization is an indication of the number of moments that are still pointing along the direction of applied field after the field is removed. Below 35K, the randomly oriented domains in the shell begin to show blocking behavior. Due to the random direction of blocking in the shell, the effective magnetization (at zero field) per nanoparticle drops which is seen as the drop in remanence. This is supported by the occurrence of a second peak (~37 K) in the ZFC cure at 2T due to blocking

of shell (not shown). Figure 6b shows the temperature dependence of distribution $f(T_B)$ or the energy barrier. The distribution $f(T_B)$ is fitted to a weighted sum of two log normal distributions given by Eq. (5).

$$f(T_B) = \frac{A}{T_B\sqrt{2\pi}\sigma_1}\exp\left(-\frac{1}{2\sigma_1^2}ln^2\frac{T}{T_1}\right) + \frac{(1-A)}{T_B\sqrt{2\pi}\sigma_2}\exp\left(-\frac{1}{2\sigma_2^2}ln^2\frac{T}{T_2}\right) \quad (5)$$

The obtained fitted parameters are T_1 = 48 K, σ_1 = 0.086, T_2 = 21 K, σ_2 = 0.33 and the weighting factor A = 0.29. The existence of two maxima in the energy barrier is consistent with our findings from Figure 5 and corroborates the fact that energy barriers E_{cr} and E_{sh} are centered about temperatures T_1 and T_2, respectively. The maximum at T_1 is at the same temperature as T_f obtained from ac susceptibility measurements. The low field ac susceptibility measurement essentially probes the dynamics of the core since it has been discussed earlier that the disordered shell is affected only at high fields (> 6 kOe). So, one can say that the freezing temperature T_f ~ 48 K as calculated from χ' corresponds to the freezing of the core ($T_{f\text{-}cr}$). Based on the same argument, the maximum at T_2 (~21 K) can be attributed to the freezing of shell ($T_{f\text{-}sh}$). This seems reliable since the freezing temperature $T_{f\text{-}sh}$ ~ 21 K is less than the mean blocking temperature of the shell (T_{B2} ~ 24 K) calculated from the AT line fit (Figure 5b). Thus, we can identify two sets of mean blocking temperatures (T_{B1}, T_{B2}) and freezing temperatures ($T_{f\text{-}cr}$, $T_{f\text{-}sh}$) for the core and the shell respectively.

All the above experiments hint to the presence of EB and so we measured M(H) hysteresis loops at 5 K under the ZFC and FC (2T) protocol. Figure 7(a) shows the M(H) loops measured under ZFC and 2 T FC conditions. EB can be confirmed by the loop shift to the negative field axis as seen for the FC case. This is accompanied by an upward shift in the loop and enhanced coercivity, which has been observed in other EB systems[10, 51-55]. The exchange bias field is calculated as H_{EB} $\left[=\frac{|(H^+ + H^-)|}{2}\right]$ where H^+ and H^- are the coercive fields for the ascending and descending curves respectively. In figure 7(b), the temperature dependence of EB field is plotted for cooling fields of 2 T and 5 T. One may argue that the onset temperature of exchange bias may depend on the magnetic field applied while cooling. So, we studied the temperature dependence of exchange bias for two different cooling fields (2 T and 5 T). In both cases, EB field starts to develop from ~ 35 K and as

temperature decreases, H_{EB} increases slowly at first, followed by a rapid increase. In the insets (Figure 7b), we have plotted the rate of change of $\frac{dH_{EB}}{dT}$ with respect to temperature, in other words $\frac{d^2H_{EB}}{dT^2}$ vs. temperature whose peak corresponds to the temperature below which EB exhibits a rapid rise. This rapid rise in EB was found to occur at 21.5 K and 20 K for cooling fields of 2 T and 5 T respectively which are in proximity to $T_{f\text{-}sh}$ (~ 21 K). From our previous discussion, at 35 K, the core is frozen with its spins aligned along the field and the shell begins to show a blocking behavior. Due to the slow dynamics of the blocked spins (< 35 K) in the shell they behave as pinning centers leading to the development of EB. This marks the onset of EB in the core-shell nanoparticles. Below 21 K (< $T_{f\text{-}sh}$), when the shell is completely frozen, the number of pinning centers increase due to enhanced exchange coupling between the core and the shell. Although the strength of the exchange coupling constant of each exchange coupled bond remains constant, this phenomenon can be attributed to the increase in density of exchange coupled bonds across the core-shell interface (i.e. number of frozen spins at the interface per unit area) and is consistent with results from previous studies[4, 56-58]. In our discussion on the magnetic state of the core and the shell, the term 'frozen' is used with respect to time scale; i.e. the collective reversal mechanism of moments in the ground state (absence of external magnetic field) occurs over a large time span (several hundred seconds). For a system to display exchange bias, there must exist at least, two exchange coupled phases: one reversible phase that can be reversed and one fixed phase that cannot be reversed in the field range of measurements[3, 7]. In the context of our core-shell nanoparticles, the fixed phase is the 'shell' and the reversible phase is the 'core'. At low temperatures below ~ 35 K, while the shell behaves as the fixed phase, the magnetization of the 'frozen' core can be reversed by application of an external field. The reversal of the core moments with respect to the shell moments leads to exchange bias which has been reported in previous studies. Below ~ 21 K, a rapid increase in EB is observed (Figure 7b), which can be explained by the same mechanism as discussed above. The enhancement in EB occurs due to increase in the number of frozen spins at the interface per unit area[56] which has been argued to develop due to freezing of the shell moments. Consistently, a rapid increase in H_{EB} is recorded below $T_{f\text{-}sh}$. So, one can conclude that in the case of core-shell nanoparticles, the onset of EB is associated with the blocking of spins in the shell while the core is in the frozen state.

IV. CONCLUSIONS

In summary, we have investigated the static and dynamic magnetic behavior of Fe/γ-Fe_2O_3 core shell nanoparticles. The nanoparticles exhibit a collective SSG type behavior below the glass transition temperature and show signs of aging. We demonstrate that the response of the core-shell nanoparticles in different low/high magnetic field regimes is different and greatly influences the mean blocking temperature. The core responds to low fields while the shell is unaffected; however at high fields, when the core is saturated, $<T_B>$ is influenced by the dynamics of the shell. The energy barrier distribution is found to have two maxima corresponding to the individual freezing of the core and shell. Finally, we have shown conclusive evidence that the onset of EB depends on the magnetic state of the core and shell. EB is found to develop at the temperature that marks the onset of shell blocking below the freezing temperature of the core. These observations opens up the possibility of tailoring EB and its onset temperature by suitably choosing different materials for the core and shell that show blocking and freezing phenomena at a desired temperature range.

ACKNOWLEDGEMENTS

The research was supported by DOE through grant number DE-FG02-07ER46438. HS also acknowledges support from the Center for Integrated Functional Materials through grant USAMRMC W81XWH-10-2-0101. MHP thanks the support from the Florida Cluster for Advanced Smart Sensor Technologies.

REFERENCES

1 R. L. Stamps, Journal of Physics D-Applied Physics **33**, R247 (2000).
2 M. Kiwi, Journal of Magnetism and Magnetic Materials **234**, 584 (2001).
3 J. Nogues and I. K. Schuller, Journal of Magnetism and Magnetic Materials **192**, 203 (1999).
4 O. Iglesias, A. Labarta, and X. Batlle, Journal of Nanoscience and Nanotechnology **8**, 2761 (2008).
5 S. Giri, M. Patra, and S. Majumdar, Journal of Physics-Condensed Matter **23**, 073201 (2011).
6 S. Laureti, S. Y. Suck, H. Haas, E. Prestat, O. Bourgeois, and D. Givord, Physical Review Letters **108**, 077205 (2012).
7 W. H. Meiklejohn and C. P. Bean, Physical Review **105**, 904 (1957).
8 A. Maitre, D. Ledue, and R. Patte, Journal of Magnetism and Magnetic Materials **324**, 403 (2012).
9 K. Nadeem, H. Krenn, T. Traussing, and I. Letofsky-Papst, Journal of Applied Physics **109**, 013912 (2011).
10 S. Karmakar, S. Taran, E. Bose, and B. K. Chaudhuri, C.P. Sun, C.L. Huang, H.D. Yang, Physical Review B **77**, 144409 (2008).
11 M. Xu, W. Zhong, J. Yu, W. Zang, C. Au, Z. Yang, L. Lv, and Y. Du, Journal of Physical Chemistry C **114**, 16143 (2010).
12 M. Ali, P. Adie, C. H. Marrows, D. Greig, B. J. Hickey, and R. L. Stamps, Nature Materials **6**, 70 (2007).
13 F.-T. Yuan, J.-K. Lin, Y. D. Yao, and S.-F. Lee, Applied Physics Letters **96**, 162502 (2010).
14 M. Gruyters, Epl **77**, 57006 (2007).
15 Q. K. Ong, A. Wei, and X.-M. Lin, Physical Review B **80**, 134418 (2009).
16 X. Sun, N. F. Huls, A. Sigdel, and S. Sun, Nano Letters **12**, 246 (2012).
17 Y. Hu and A. Du, Journal of Applied Physics **110**, 1967 (2011).
18 H. Khurshid, V. Tzitzios, W. Li, C. G. Hadjipanayis, and G. C. Hadjipanayis, Journal of Applied Physics **107**, 09A333 (2010).
19 A. Cabot, A. P. Alivisatos, V. F. Puntes, L. Balcells, O. Iglesias, and A. Labarta, Physical Review B **79**, 094419 (2009).
20 M. Suzuki, S. I. Fullem, I. S. Suzuki, L. Wang, and C.-J. Zhong, Physical Review B **79**, 024418 (2009).
21 C. R. Lin, R. K. Chiang, J. S. Wang, and T. W. Sung, Journal of Applied Physics **99**, 08N710 (2006).
22 L. He, Solid State Communications **150**, 743 (2010).
23 J. L. Dormann, D. Fiorani, and E. Tronc, Journal of Magnetism and Magnetic Materials **202**, 251 (1999).
24 S. Pal, S. Chandra, M.-H. Phan, P. Mukherjee, and H. Srikanth, Nanotechnology **20**, 485604 (2009).
25 J. D. Moore, G.K. Perkins, K. Morrison, L. Ghivelder, M.K. Chattopadhyay, S.B. Roy, P. Chaddah, Jr. A.K. Gschneidner, V.K. Pecharsky, and L.F. Cohen, Journal of Physics-Condensed Matter **20**, 465212 (2008).
26 G. P. Zheng and J. X. Zhang, Journal of Physics-Condensed Matter **10**, 275 (1998).
27 K. De, S. Majumdar, and S. Giri, Journal of Applied Physics **101**, 103909 (2007).
28 J. A. Mydosh, *Spin Glasses: An Experimental Introdution* (Taylor and Francis, London, 1993).
29 X. Chen, S. Bedanta, O. Petracic, W. Kleemann, S. Sahoo, S. Cardoso, and P. P. Freitas, Physical Review B **72**, 214436 (2005).
30 K. Binder and A. P. Young, Physical Review B **29**, 2864 (1984).
31 C. Djurberg, P. Svedlindh, P. Nordblad, M. F. Hansen, F. Bodker, and S. Morup, Physical Review Letters **79**, 5154 (1997).
32 M. Sasaki, P. E. Jonsson, H. Takayama, and H. Mamiya, Physical Review B **71**, 104405 (2005).

[33] R. K. Zheng, H. W. Gu, and X. X. Zhang, Physical Review Letters **93**, 139702 (2004).
[34] D. S. Fisher and D. A. Huse, Physical Review B **38**, 386 (1988).
[35] D. S. Fisher and D. A. Huse, Physical Review B **38**, 373 (1988).
[36] J. Alonso, M. L. Fdez-Gubieda, J. M. Barandiaran, A. Svalov, L. Fernandez Barquin, D. Alba Venero, and I. Orue, Physical Review B **82**, 054406 (2010).
[37] H. M. Nguyen, D. H. Manh, L. V. Hong, N. X. Phuc, and Y. D. Yao, Journal of the Korean Physical Society **52**, 1447 (2008).
[38] P. Allia, M. Coisson, P. Tiberto, F. Vinai, M. Knobel, M. A. Novak, and W. C. Nunes, Physical Review B **64**, 144420 (2001).
[39] J. C. Denardin, A. L. Brandl, M. Knobel, P. Panissod, A. B. Pakhomov, H. Liu, and X. X. Zhang, Physical Review B **65**, 064422 (2002).
[40] X. X. Zhang, H. L. Wei, Z. Q. Zhang, and L. Y. Zhang, Physical Review Letters **87**, 157203 (2001).
[41] S. Morup and E. Tronc, Physical Review Letters **72**, 3278 (1994).
[42] H. Khurshid, W. Li, V. Tzitzios, and G. C. Hadjipanayis, Nanotechnology **22**, 265605 (2011).
[43] B. Mehdaoui, A. Meffre, L. M. Lacroix, J. Carrey, S. Lachaize, M. Respaud, M. Gougeon, and B. Chaudret, Journal of Applied Physics **107**, 09A324 (2010).
[44] T. Jonsson, J. Mattsson, C. Djurberg, F. A. Khan, P. Nordblad, and P. Svedlindh, Physical Review Letters **75**, 4138 (1995).
[45] K. Binder and A. P. Young, Reviews of Modern Physics **58**, 801 (1986).
[46] L. E. Wenger and J. A. Mydosh, Physical Review B **29**, 4156 (1984).
[47] G. Kotliar and H. Sompolinsky, Physical Review Letters **53**, 1751 (1984).
[48] N. deCourtenay, A. Fert, and I. A. Campbell, Physical Review B **30**, 6791 (1984).
[49] R. W. Chantrell, M. Elhilo, and K. Ogrady, Ieee Transactions on Magnetics **27**, 3570 (1991).
[50] C. P. Bean, J. D. Livingston, and D. S. Rodbell, Journal De Physique Et Le Radium **20**, 298 (1959).
[51] H. M. Nguyen, P.-Y. Hsiao, and M.-H. Phan, Journal of Applied Physics **107**, 09D706 (2010).
[52] K. Nadeem and H. Krenn, Journal of Superconductivity and Novel Magnetism **24**, 717 (2011).
[53] B. Martinez, X. Obradors, L. Balcells, A. Rouanet, and C. Monty, Physical Review Letters **80**, 181 (1998).
[54] T. N. Shendruk, R. D. Desautels, B. W. Southern, and J. van Lierop, Nanotechnology **18**, 455704 (2007).
[55] R. K. Zheng, G. H. Wen, K. K. Fung, and X. X. Zhang, Physical Review B **69**, 214431 (2004).
[56] Q. K. Ong, X.-M. Lin, and A. Wei, Journal of Physical Chemistry C **115**, 2665 (2011).
[57] O. Iglesias, X. Batlle, and A. Labarta, Physical Review B **72**, 212401 (2005).
[58] E. Eftaxias and K. N. Trohidou, Physical Review B **71**, 134406 (2005).

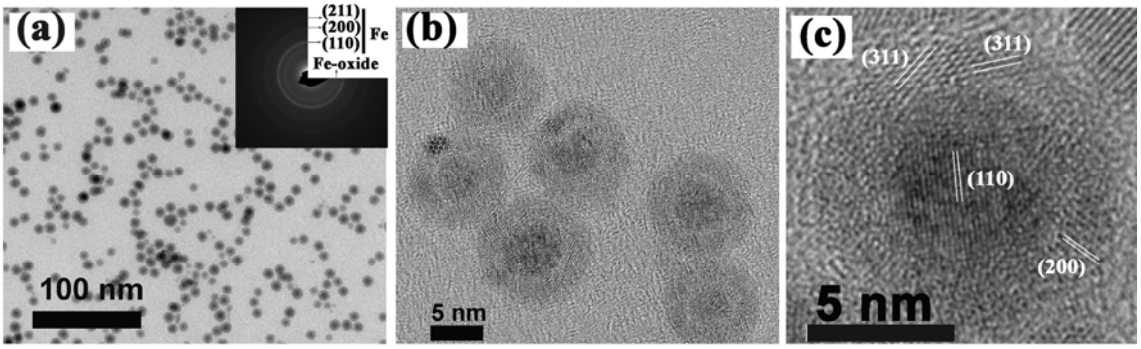

(Color online) FIG 1. Bright field (a) TEM and (b,c) HRTEM images of Fe/γ-Fe_2O_3 core-shell nanoparticles. Inset 1(a) shows selected area diffraction pattern.

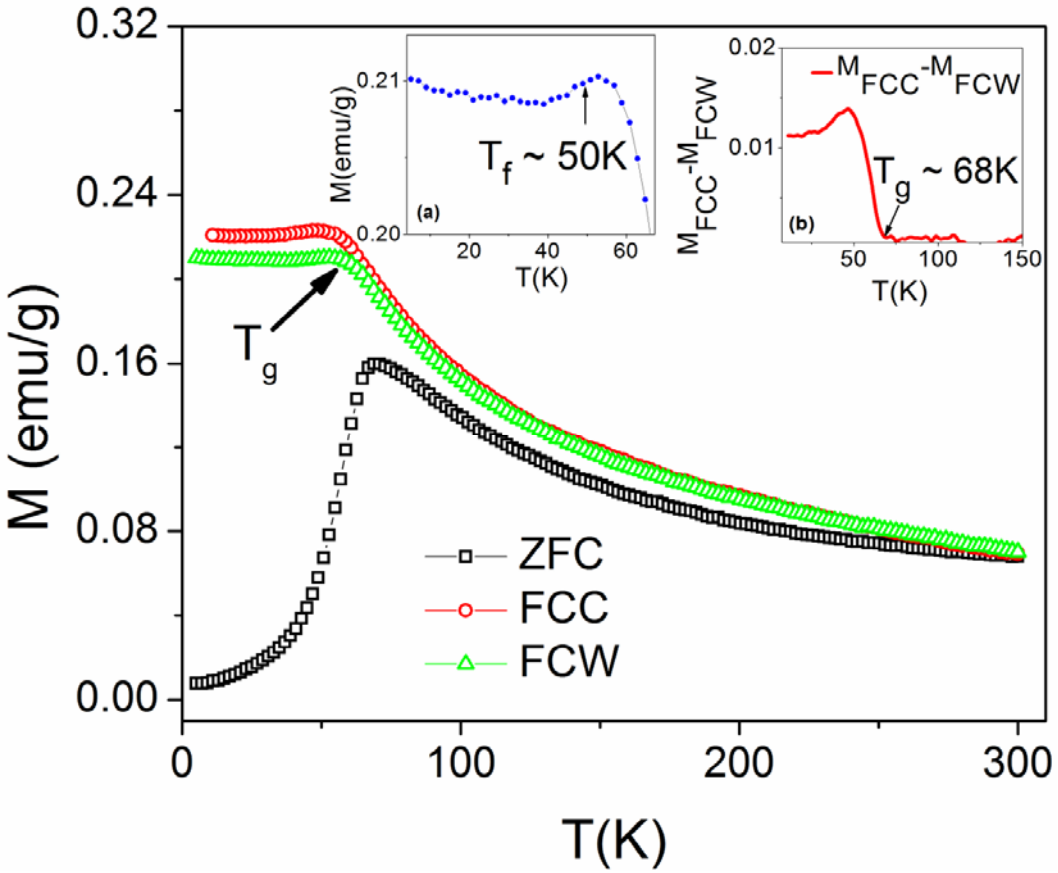

(Color online) FIG 2. Temperature dependence of magnetization for zero-field cool (ZFC), field cool-cooling (FCC) and field cool-warming (FCW). Inset (a) the dip in M_{FCW} is associated with onset of spin freezing (T_f ~ 50K); and (b) shows the difference (M_{FCC}-M_{FCW}) plotted against temperature, where a sharp rise (T_g ~ 68K) marks the onset of thermal hysteresis.

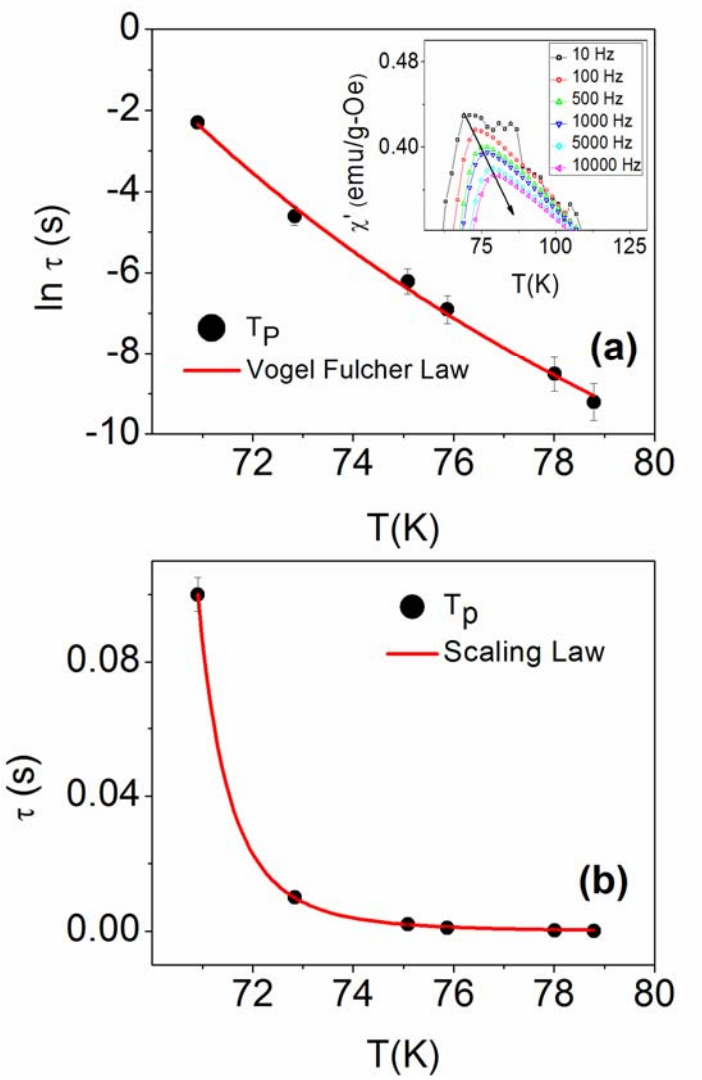

(Color online) FIG 3. The best fit of the relaxation times (τ) to (a) the Vogel-Fulcher law and (b) the scaling law. Inset shows the frequency dependence of peak temperature (T_P) in χ'.

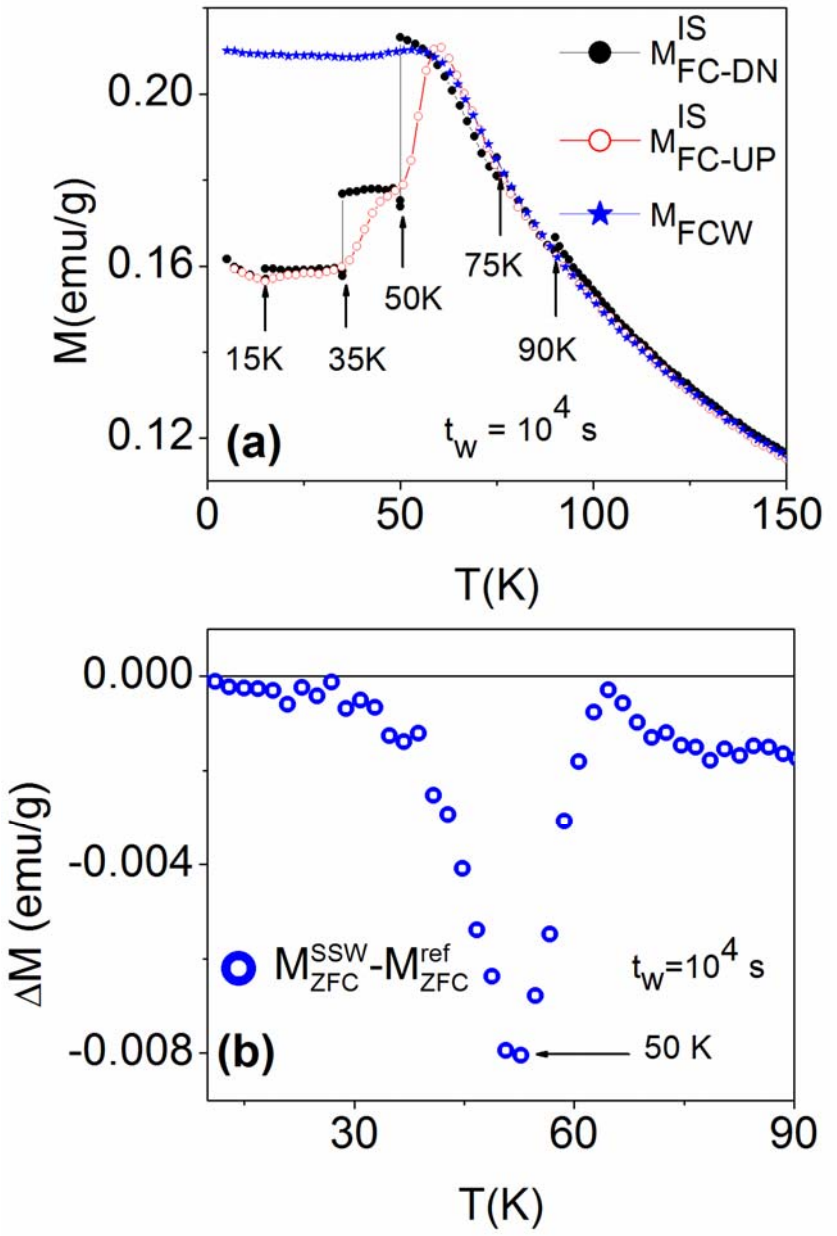

(Color online) FIG 4. (a) Temperature dependence of M^{IS}_{FC-DN} and M^{IS}_{FC-UP} observed in the FC aging protocol and (b) Temperature dependence of $(M^{SSW}_{ZFC} - M^{ref}_{ZFC})$ in the ZFC aging protocol.

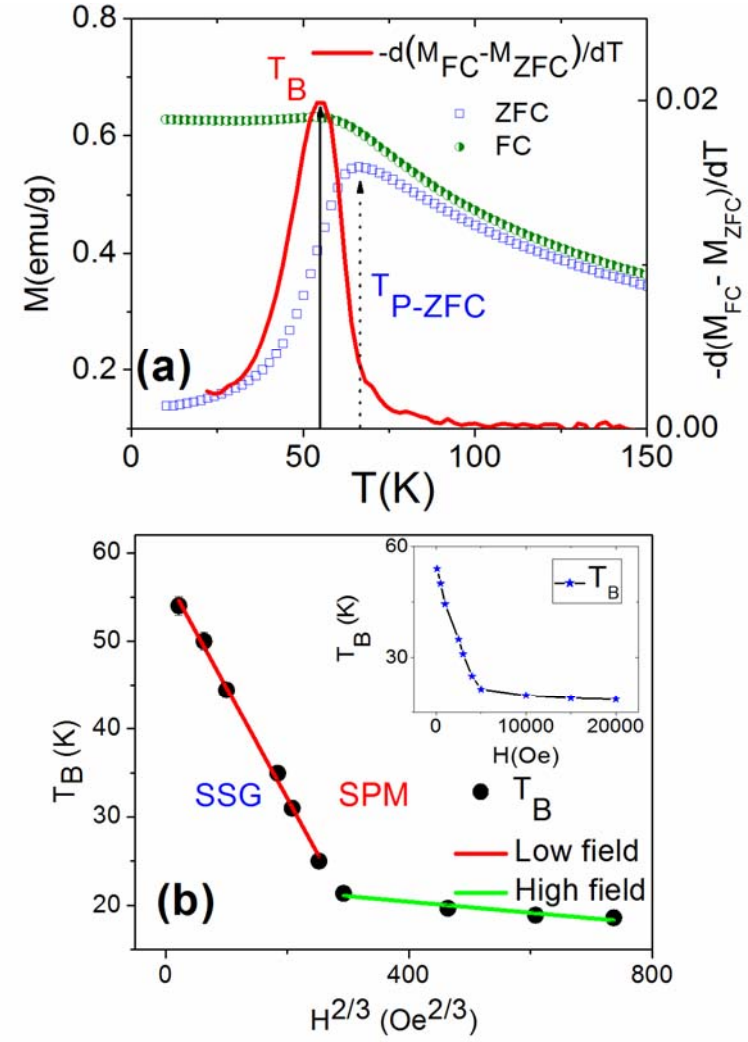

(Color online) FIG 5. (a) ZFC/FC curve and the derivative d $[M_{FC}-M_{ZFC}]/dT$ indicating peak temperature of M_{ZFC} (T_{pk}) and mean blocking temperature (T_B); (b) Two straight AT-line fits for low and high field regime. Inset shows the evolution of blocking temperature (T_B) with measurement field.

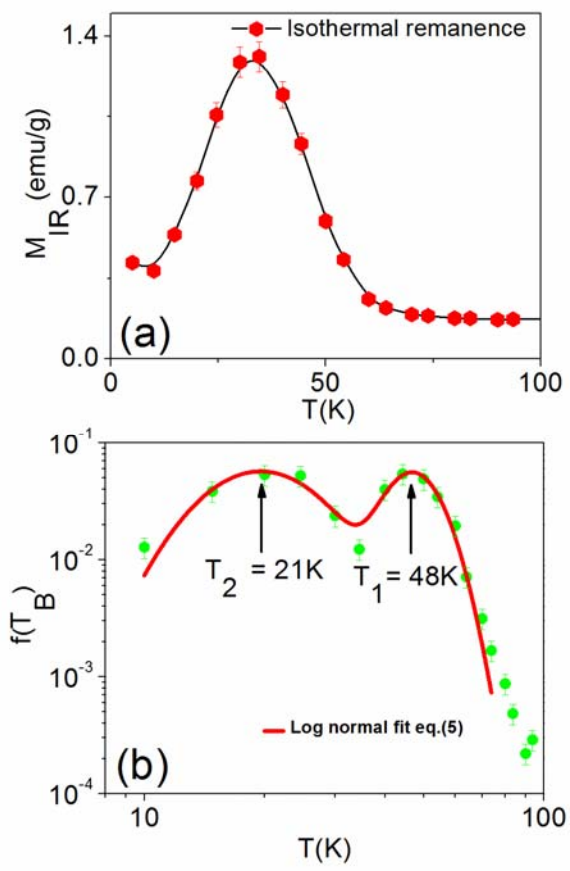

(Color online) FIG 6. (a)Temperature dependence of isothermal remanence, (b) Distribution function fit to Eq. (5)

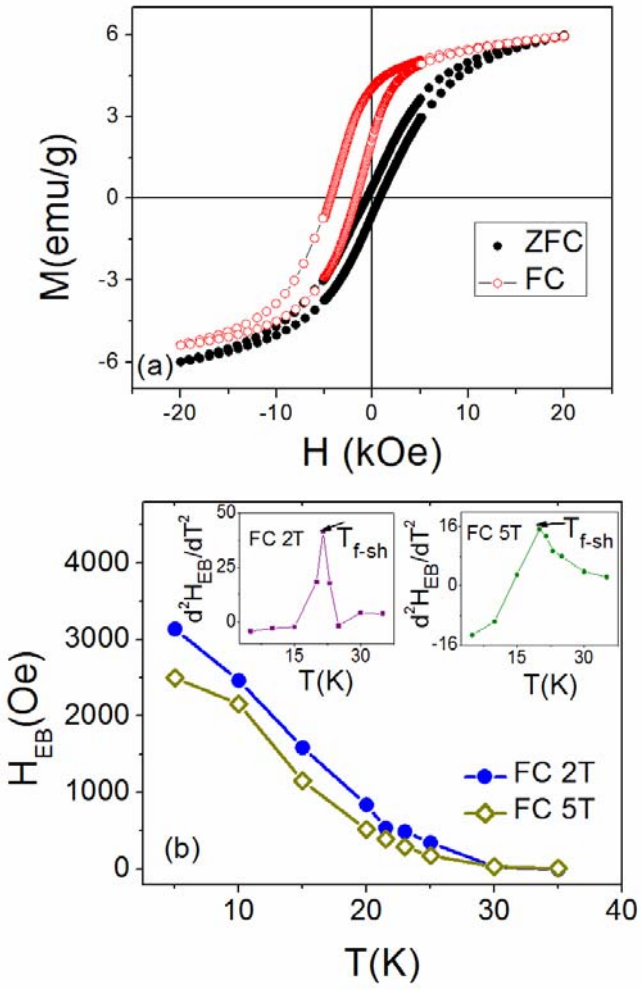

(Color online) FIG 7. (a) M-H hysteresis loops at 5K under FC (2T) and ZFC conditions, (b) temperature dependence of exchange bias field measured for cooling magnetic fields of 2 T and 5 T. Insets show the $\frac{d^2H_{EB}}{dT^2}$ vs. T curves for cooling magnetic fields of 2T and 5T.